Chinese Chemical Letters 36 (2025) 109920

Contents lists available at ScienceDirect

Chinese Chemical Letters

journal homepage: www.elsevier.com/locate/cclet

Facile synthesis of phenazine-conjugated polymer material with extraordinary proton-storage redox capability

Renyuan Wang[a,1], Lei Ke[c,1], Houxiang Wang[a], Yueheng Tao[a], Yujie Cui[a], Peipei Zhang[a], Minjie Shi[a,d,*], Xingbin Yan[b,*]

[a] School of Materials Science and Engineering, Jiangsu University of Science and Technology, Zhenjiang 212003, China
[b] School of Materials Science and Engineering Sun Yat-sen University, Guangzhou 510275, China
[c] Jiangsu Hilong Technology Co., Ltd., Zhenjiang 212003, China
[d] College of Chemistry and Molecular Sciences, Wuhan University, Wuhan 430072, China

ARTICLE INFO

Article history:
Received 29 February 2024
Revised 15 April 2024
Accepted 23 April 2024
Available online 24 April 2024

Keywords:
Aqueous battery
Molecular design
Organic material
Proton storage
Electrochemical mechanism

ABSTRACT

Aqueous proton batteries (APBs) embody a compelling alternative in the realm of economical and reliable energy technologies by virtue of their distinctive "Grotthuss mechanism". Sustainable production and adjustable molecular structure make organic polymers a promising choice for APB electrodes. However, inadequate proton-storage redox capability currently hinders their practical implementation. To address this issue, we introduce a pioneering phenazine-conjugated polymer (PPZ), synthesized through a straightforward polymerization process, marking its debut in APB applications. The inclusion of *N*-heteroaromatic fused-ring in the extended π-conjugated framework not only prevents the dissolution of redox-active units but also refines the energy bandgap and electronic properties, endowing the PPZ polymer with both structural integrity and enhanced redox activity. Consequently, the PPZ polymer as an electrode material achieves a remarkable proton-storage capacity of 211.5 mAh/g, maintaining a notable capacity of 158.3 mAh/g even under a high rate of 8 A/g with a minimal capacity fade of merely 0.00226% per cycle. The rapid, stable and impressive redox behavior is further elucidated through *in-situ* techniques and theoretical calculations. Ultimately, we fabricate an APB device featuring satisfactory electrochemical attributes with an extraordinary longevity over 10,000 cycles, thereby affirming its auspicious potential for eminent applications.

Choosing the appropriate electrochemical system to efficiently store energy from renewable sources like solar and wind is essential for reaching carbon reduction targets [1–3]. Within the realm of such systems, aqueous batteries stand out as dependable options for extensive energy storage due to their benign environmental impact, ease of construction and affordability [4,5]. However, aqueous batteries, which employ single-valence (Li^+, Na^+, K^+) and multiple-valence (Mg^{2+}, Ca^{2+}, Zn^{2+}, Al^{3+}) metal ions, are frequently plagued by slow ion movement because of their intense electrostatic forces and the energy barrier to remove their hydration shell [6–8]. Proton, a simplest and lightest charge carrier on the periodic table, is exceptional in its ability to conduct quickly in aqueous environments *via* a process defined by the distinctive "Grotthuss mechanism" [9–11]. Moreover, proton has the potential to form covalent or ionic linkages with diverse organic and inorganic entities, greatly enhancing the scope for creating innovative electrode materials. Thus, the pursuit of electrodes designed to accommodate proton is regarded as a strategic pathway in the advancement of efficient aqueous proton batteries (APBs).

The advancement of APBs hinges on creating cutting-edge electrode materials that are not only electrochemically reliable but also safe, eco-conscious and economically viable. Organic compounds, sourced from copious natural resources, have arisen as contenders to replace the conventionally utilized inorganic compounds, favored for their high theoretical capacity, structural variability, environmental compatibility and minimal ecological impact [12,13]. Organic compounds, when assembled *via* van der Waals interactions, present flexible and spacious structural matrixes that can accommodate the volumetric changes during the electrochemical process [14,15]. Crucially, the structural versatility of the organic compounds allows for a broader range of electrode design possibilities. However, significant obstacles impeding advancement include their inherently poor electronic conductivity and low re-

* Corresponding authors.
E-mail addresses: shiminjie@just.edu.cn (M. Shi), yanxb3@mail.sysu.edu.cn (X. Yan).
[1] These authors contributed equally to this work.

https://doi.org/10.1016/j.cclet.2024.109920
1001-8417/

dox stability [16,17]. When used as proton-storage electrodes, the redox-active organic compounds are susceptible to leaching into the aqueous electrolytes, which drastically shorten their cycle life and negate the benefits of their high initial capacities. Additionally, the inherently low conductive nature of most organic compounds requires the incorporation of a substantial quantity of conductive additives during electrode fabrication, thereby severely diminishing the practical energy density of assembled APB devices.

The polymerization of redox-active molecules is a proven strategy to counteract the dissolution of organic compounds, while the incorporation of heteroatoms (O, N and S) into organic compounds to form π-conjugated aromatic structure can introduce multiple redox centers and boost the intrinsic electrical conductivity [18,19]. It is worth noting that the difference between imine and carbonyl polymers is that the imine group contains lone pair electrons. These electrons are crucial for enhancing the electrochemical activity of imine polymer through redox reactions within the electrode. In addition, imine polymers are largely neutral organic bases and have a natural affinity for proton storage [20,21]. Motivated by these insights, we have developed a new N-heteroaromatic imine phenazine-based polymer (PPZ) featuring an extended π-conjugated framework to enhance the density of redox-active sites and overall structural robustness. Notably, the PPZ polymer can be synthesized *via* a straightforward polymerization reaction under facile and mild conditions. Utilized as an electrode material, the PPZ polymer offers a substantial proton-storage capacity, registering 211.5 mAh/g at a current density of 1 A/g, and maintains impressive rate performance along with remarkable long-term stability with a minimal capacity fade rate of only 0.00226% each cycle. *In-situ* dynamic analysis and theoretical calculations have uncovered a quick and reversible redox mechanism during proton uptake and release. Additionally, a soft-package APB device with the PPZ electrode showcases an impressive energy density of 68.68 Wh/kg and a power density of 8500 W/kg, while maintaining an exceptional operational lifespan over 10,000 cycles, thus underscoring its significant potential for real-world application scenarios.

The PPZ polymer was produced using a straightforward one-step polymerization process involving phenazin-1-ylamine (PZM) monomer and $(NH_4)_2S_2O_8$ oxidant under relatively benign conditions of 79 °C, as detailed in the experimental section of the Supporting Information. This synthesis method is uncomplicated and does not necessitate sophisticated equipment. The precursor materials are economical, rendering it feasible for scaling up to industrial levels. As depicted in Fig. 1a, the scanning electron microscope (SEM) of the PPZ polymer exposes minuscule particles, and the elemental analysis images that accompany it validate a uniform distribution of C and N elements within the polymer matrix. The ^{13}C NMR spectrum of the PPZ polymer in its solid state (Fig. 1b), reveals distinctive peaks at specific chemical shifts. A peak at 144.8 ppm corresponds to carbon atoms in C=N bonds (depicted in purple), while two peaks at 142.2 and 134.3 ppm indicate carbon atoms in C=C bonds (marked in red and green) [22,23]. Furthermore, two peaks at 129.3 and 122.9 ppm represent carbon atoms in C-C bonds (shown in orange and blue), originating from the benzene rings in the polymer structure. The X-ray diffraction (XRD) patterns of the PZM monomer and PPZ polymer are compared in Fig. 1c, with the polymer exhibiting a diffraction peak at approximately 26.7°. This broad peak indicates the robust π-π interactions among the imine heterocycles intertwined within the PPZ polymer matrix. The results of thermal stability evaluations conducted using thermal gravimetric analysis (TGA) on the PZM monomer and PPZ polymer are illustrated in Fig. 1d. The analysis reveals that the PPZ polymer decomposes at a higher temperature (500 °C) with minimal weight loss (80.6%), indicating its robust polymeric structure. The PPZ polymer is subjected to additional analysis by using X-ray photoelectron spectroscopy (XPS) (Fig. 1e).

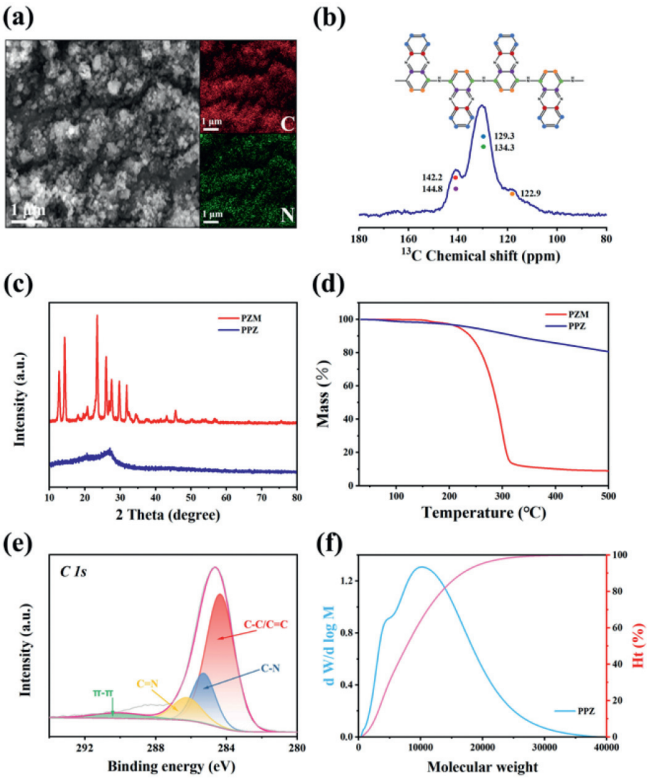

Fig. 1. Structural characterizations of the PPZ polymer. (a) SEM image and elemental analysis images, (b) solid-state ^{13}C NMR spectrum, (c) XRD pattern, (d) TGA curve, (e) C 1s XPS spectrum and (f) distribution curve of molecular weight of the PPZ polymer.

Several signals at 284.4, 285.2 and 286.5 eV are indicative of carbon atoms involved in C–C/C=C, C-N, and C=N bonds, respectively. Furthermore, a prominent signal observed at 290.5 eV can be attributed to the π-π interactions that occur between PPZ molecules [24]. The degree of polymerization of PPZ polymer was evaluated by gel permeation chromatography (GPC) test. Fig. 1f shows the distribution curve related to the molecular weight of the PPZ polymer, with an average molecular weight of ~9.1 kDa. For more information on the structural characterizations of the PPZ polymer, please refer to Figs. S1-S3 (Supporting information).

A comprehensive three-electrode study was firstly conducted to examine the electrochemical properties of the PPZ polymer when deployed as an electrode substance in an aqueous medium of 1 mol/L H_2SO_4 solution. Fig. 2a showcases the cyclic voltammetry (CV) profiles of the PPZ electrode at varying sweep rates, showing clear and unaltered redox peaks. The *b* values for the redox peaks in Fig. 2b are determined to be 0.83 and 0.88, suggesting the presence of diffusion- and capacitive-controlled steps in the redox processes of the PPZ electrode [25]. The Trasatti analysis was used to objectively distinguish between diffusion- and capacitive-controlled contributions. Fig. 2c delineates an escalation in the capacitive-controlled contribution concomitant with the augmentation of sweep rates, hence illustrating the enhanced rate capability of the PPZ electrode. The related calculation process of the capacitive contributions is provided in Fig. S4 (Supporting information). The nonlinear morphologies observed in the galvanostatic charge/discharge (GCD) profiles (Fig. 2d) further elucidate the redox behaviors of the PPZ electrode. The PPZ electrode provides a large specific capacity of 211.5 mAh/g at a current density of 1 A/g, which is 76.6% of the theoretical capacity (275.99 mAh/g, detail in supplementary material), in conjunction with impressive specific capacities of 158.3 and 125.3 mAh/g

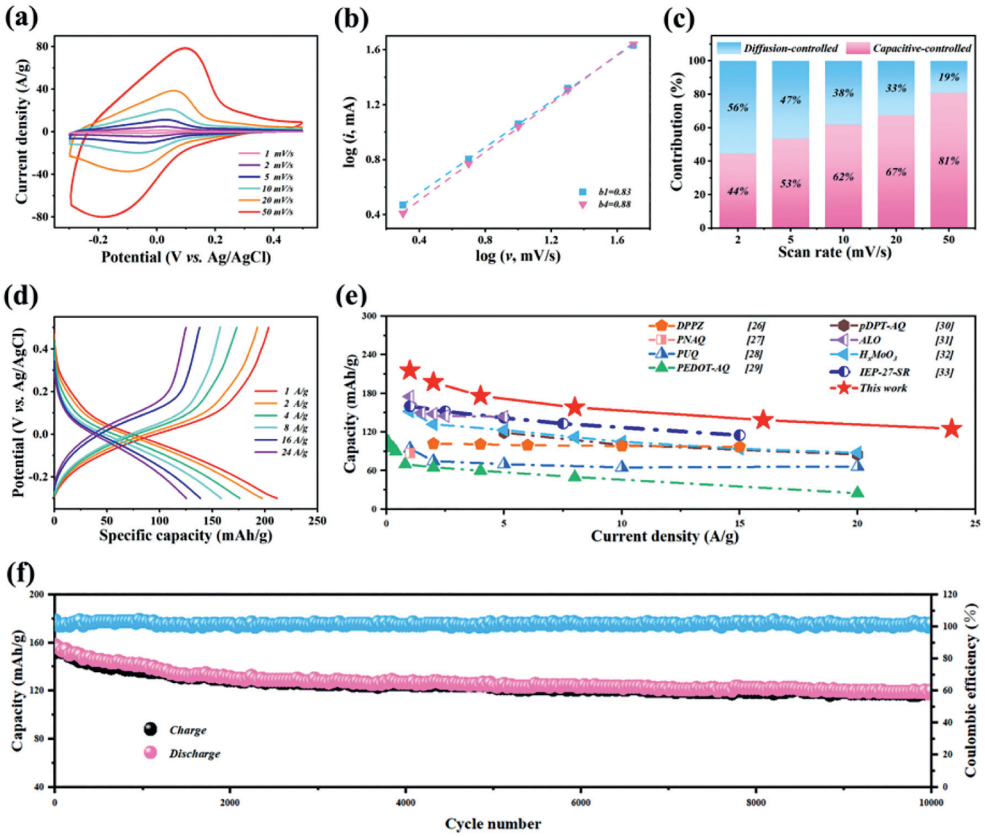

Fig. 2. Electrochemical properties of the PPZ electrode in 1 mol/L H_2SO_4 electrolyte. (a) CV curves, (b) *b* values and (c) the corresponding capacity contributions at various scan rates from 1 mV/s to 50 mV/s. (d) GCD curves ranging from 1 A/g to 24 A/g. (e) Rate performance comparison to the reported proton-storage electrodes. (f) Cycle stability and coulombic efficiency over 10,000 repeated charging/discharging cycles at 8 A/g.

at elevated loading densities of 8 and 24 A/g, which speaks to its exceptional rate performance when compared with advanced proton-storage electrodes (Fig. 2e and Table S1 in Supporting information) previously reported [26–33]. Fig. 2f illustrates the cycle durability and coulombic efficiency of the PPZ electrode during 10,000 cycles at 8 A/g. showcasing a remarkably long lifespan and a low deterioration rate of about 0.00226% each cycle in terms of average capacity. The expanded π-conjugated architecture of the PPZ electrode fortifies its durability by diminishing its solvency within the aqueous electrolyte. As shown in Fig. S5 (Supporting information), the PPZ electrode exhibits nearly 100% coulombic efficiency when subjected to continuous charge/discharge cycles, demonstrating its high redox reversibility for proton storage. *In-situ* UV–vis spectroscopy (Fig. S6 in Supporting information) shows the electrolyte conditions without obvious dissolution phenomenon of the PPZ electrode upon charging and discharging. By contrast, the PZM monomer as electrode material shows poor cycling durability with a 41% capacity retention after 140 cycles (Fig. S7 in Supporting information), which is attributed to its high solubility in acidic aqueous electrolyte.

Electrochemical impedance spectroscopy (EIS) provides the electrochemical characteristics of the PPZ electrode. The electrical resistance within the bulk material (R_s) and the impedance to charge migration at the interface (R_{ct}) are both exceptionally minimal, with R_s at 0.16 Ω and R_{ct} at 2.02 Ω, signifying an expeditious electrochemical reaction with negligible obstruction within the PPZ electrode. The proton diffusion coefficient (D) can be calculated by using the Warburg factor according to the classical equation [34]. As shown in Fig. 3b, the D value calculated for the PPZ electrode is as low as 4.53×10^{-7} cm^2/s, indicating the efficient ionic diffusion within the PPZ electrode. The polymer chain of the PPZ polymer is not rigidly fixed, allowing it to regulate and respond to ionic movements. Even with a three-dimensional framework, the polymer chain is capable of conformational evolution when exposed to the external stimuli, thereby creating transient pathways that facilitate ion transport. Additionally, the three-dimensional internal structure of the PPZ polymer displays some available pores that significantly facilitate ion permeation. Furthermore, the D values at various temperatures was used to determine the activation energy for proton diffusion. A linear association is established between the logarithm of D and T^{-1} in Fig. 3c, confirming the suitability of the Arrhenius equation $\ln(D) = -E_a/RT + C$ [35]. The calculated activation energy (E_a) of 227.9 meV is indicative of a rapid Grotthuss process, which is characteristically less than 400 meV [36]. Consequently, it is revealed that the proton diffusion efficiency of the PPZ electrode can be amplified by the "Grotthus mechanism", allowing for rapid proton jumps in the aqueous electrolyte. The 45° phase angle in the Bode plot (Fig. 3d) corresponds to an eigenfrequency (f_0) of approximately 0.5 Hz. The PPZ electrode demonstrates a rapid frequency response (τ_0) of 2.0 s, reflecting its high redox reaction for proton storage. The excellent electron-transfer ability of PPZ polymer is largely attributed to its extended π-conjugated configuration. This extended conjugation allows electrons to effectively delocalize on the polymeric backbone, facilitating the movement of charge carriers. As electrons can move more freely along the polymeric chain, the electrical conductivity of the PPZ polymer is significantly enhanced. According to the standard four-point probe technique, it is found that the PPZ polymer possesses a higher electric conductivity ($\sim 4.9 \times 10^{-2}$ S/cm) than the PZM monomer ($\sim 5.6 \times 10^{-5}$ S/cm). In addition, the N-heteroaromatic phenazine-based units within the PPZ polymeric backbone to create multiple proton conduction pathways, which leverage the distinctive

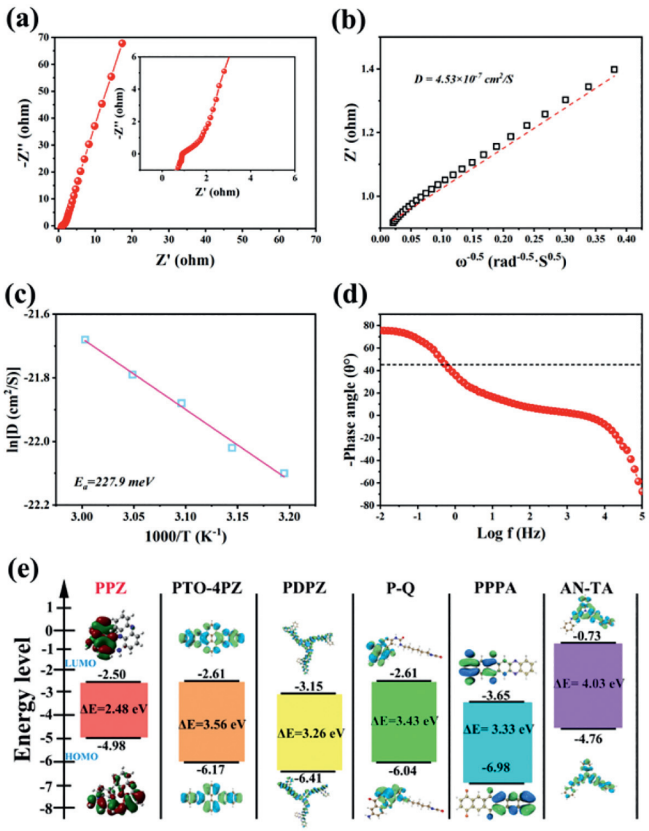

Fig. 3. Kinetic analysis of the PPZ electrode. (a) EIS plot and (b) the corresponding *D* value. (c) Plot of ln(*D*) against 1000/*T*. (d) Bode plot of the PPZ electrode. (e) Frontier molecular orbital energy of the PPZ electrode compared with other polymers for proton storage.

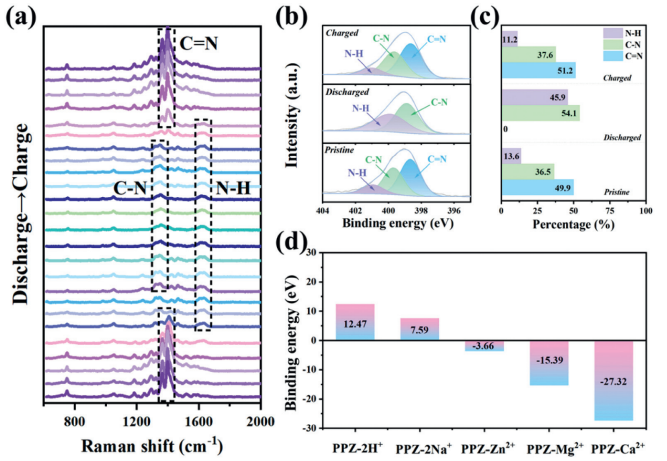

Fig. 4. Proton-storage mechanism of the PPZ electrode. (a) *In-situ* Raman spectra of the PPZ electrode upon discharging and charging. (b) *Ex-situ* XPS spectra of N 1s and (c) the corresponding percentage contents of C=N, C-N and N-H bonds. (d) Comparison of the adsorption energies of different charge carriers coordinated with PPZ molecule.

electron-rich characteristics of the imine rings. Through the Grotthuss mechanism, protons can jump from one nitrogen site to the next, facilitated by the presence of adjacent electron-rich regions within the PPZ polymer. Therefore, the heteroaromatic imine rings contain nitrogen atoms in the PPZ polymer that can act as proton relays, enabling the fast transfer of protons *via* hydrogen bonding interactions. As shown in Fig. S8 (Supporting information), the LUMO level of the PPZ polymer (−2.50 eV) is lower than that of PZM monomer (−2.43 eV), indicating the superior electron affinity of the PPZ polymer for proton storage. Additionally, the PPZ electrode possesses a narrower HOMO-LUMO gap (2.48 eV) than those of other polymer electrodes for proton storage (Fig. 3e), highlighting the superior electronic conductivity and redox kinetics of the PPZ electrode [28,37-40].

An *in-situ* Raman analysis (Fig. S9 in Supporting information) was conducted to dynamically investigate the proton coordination in the PPZ electrode. Fig. 4a displays a prominent peak at 1405 cm^{-1}, suggesting the existence of C=N bonds in the nitrogen-containing heterocycles of the PPZ electrode. The vibration intensity of the C=N bonds decreases gradually during discharge, while the signals of the C-N (1346 cm^{-1}) and N-H (1618 cm^{-1}) bonds increase progressively. The C=N bonds in the PPZ electrode are converted to the C-N bonds, which then react with protons to create the N-H bonds. The vibration intensities of the C-N and N-H bonds fall and then increase again during the following charge process, while the peaks related to the C=N bonds become visible once more. This suggests that protons are effectively removed from the PPZ electrode during oxidation processes to regenerate the C=N bonds. Besides, *ex-situ* XPS examination was performed on the PPZ electrode in its original, completely discharged and charged conditions (Fig. 4b). The detailed peak division results of the N 1s spectra are presented in Fig. 4c. Obviously, the peak intensities of N–H and C–N bonds increase after full discharge, while the peak intensity of C=N bonds completely disappears. Upon the recovery of potential, the peak intensity of C=N bonds can be restored to its initial level. This phenomenon reveals the reversible redox process that took place in the PPZ electrode (C=N ↔ C-N/N-H) during proton uptake/removal. The proposed electrochemical conversion mechanism of the PPZ electrode upon proton uptake/removal is shown in Fig. S10 (Supporting information). Fig. 4d shows that the Gibbs free energy (-Δ*G*) for the binding of the PPZ molecule to protons is calculated to be −12.47 eV, which is notably lower than the values for monovalent or multivalent metallic ions (Na^+, Zn^{2+}, Mg^{2+}, and Ca^{2+}) in aqueous electrolytes, further suggesting the strongest coordination of the protons with the PPZ electrode.

To accommodate practical applications, a stratified architecture was employed in the construction of an all-polymer APB device (Fig. 5a), which is realized by using PPZ polymer as anode and poly(indole) polymer as cathode (Fig. S11 in Supporting information). It should be noted that in order to match with the PPZ anode material, poly(indole) polymer was chosen as the cathode material for fabricating full cell. As a conductive polymer, the poly(indole) polymer possesses slower rate of hydrolysis and degradation in solution, higher electrochemical activity and better thermal stability when compared with other conductive polymers [41–43]. More importantly, it is known that the poly(indole) polymer exhibits higher redox potentials than some typical proton conduction systems such as polyaniline and polypyrrole [44,45], making it more suitable as cathode material for proton storage. The CV profiles of the fabricated APB (Fig. 5b), exhibit a wide potential window extending from 0 to 1.7 V. The APB device manifests a pair of distinct redox peaks, which retain their definition even under elevated scan rates, implying the occurrence of rapid redox process. Furthermore, the GCD profiles of the APB device (Fig. 5c), are depend on the combined weights of the cathode and anode, which delivers a high specific capacity of 81.1 mAh/g when operating at a current density of 1 A/g. As illustrated in Fig. 5d, the APB device can attain high energy density levels at various power outputs. Specifically, it provides a maximum energy density of 68.68 Wh/kg at a power density of 856 W/kg, and a maximum power density of 8500 W/kg at 30.34 Wh/kg based on the weights of cathode and anode, surpassing the performance of previously reported APB devices [28,46-51]. It is significant that the APB device retains a high capacity of ~91.7% with a coulombic efficiency approaching 100%

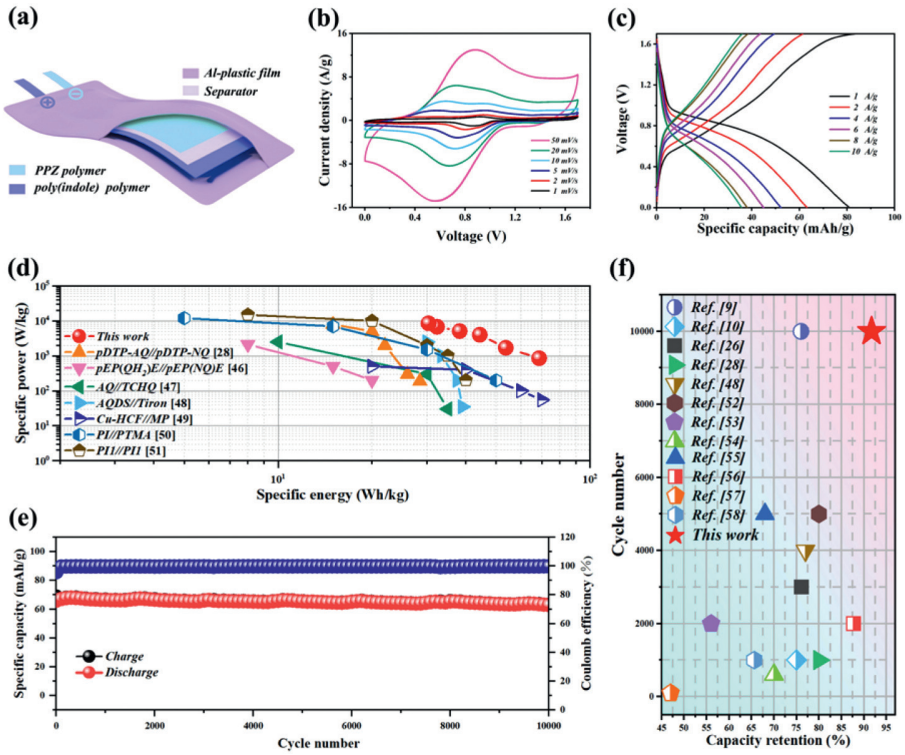

Fig. 5. Full-cell assembly and testing. (a) Device structure of the soft-package APB. (b) CV curves and (c) GCD profiles, (d) Ragon plot of the soft-package APB device based on the whole mass of anode and cathode. (e) Long-term cycle stability with coulombic efficiency at 2 A/g. (f) Cycle performance comparisons of our fabricated APB with previously reported APB devices.

even after 10,000 cycles of discharging and charging (Fig. 5e). The APB device demonstrates an extraordinary long-term stability with commendable reversibility, markedly surpassing the performance of previously reported APB devices, as evidenced by Fig. 5f and Table S2 (Supporting information) [9,10,26,28,48,52-58]. Therefore, the fabricated APB device clearly establishes its potential to meet various needs in the field of safe, reliable and efficient energy storage systems.

In summary, we have developed an innovative phenazine-based polymer with heteroaromatic and extended π-conjugated framework *via* a facile and mild polymerization approach. This well-designed configuration enhances the molecular rigidity and aromaticity, while also optimizing the electronic structure and narrowing the energy bandgap to improve the electron affinity for exceptional proton storage. Consequently, the synthesized polymer, when deployed as an electrode material, demonstrates remarkable electrochemical attributes with a high specific capacity of 211.5 mAh/g at 1 A/g, a sustained cycle stability over 6000 repetitions and a significant rate capability. Comprehensive experimental analyses, *in-situ* observations and theoretical calculations have disclosed the rapid, stable and impressive redox behavior of the polymer electrode during proton uptake and release. For practical applications, we have constructed a full-cell APB device with dependable electrochemical traits, including noteworthy energy/power densities and extended cycle life. Our findings offer new insights into the development of eco-friendly polymer electrodes for cost-effective and high-performance rechargeable aqueous batteries.

Declaration of competing interest

The authors declare that they have no known competing financial interests or personal relationships that could have appeared to influence the work reported in this paper.

CRediT authorship contribution statement

Renyuan Wang: Writing – original draft, Investigation, Data curation. **Lei Ke:** Methodology, Investigation, Formal analysis. **Houxiang Wang:** Project administration, Formal analysis. **Yueheng Tao:** Investigation, Formal analysis. **Yujie Cui:** Project administration, Methodology. **Peipei Zhang:** Writing – original draft, Validation. **Minjie Shi:** Writing – review & editing, Resources. **Xingbin Yan:** Writing – review & editing, Resources.

Acknowledgments

This work was supported by the National Natural Science Foundation of China (No. 52002157), and the China Postdoctoral Science Foundation (No. 2023M741471).

Supplementary materials

Supplementary material associated with this article can be found, in the online version, at doi:10.1016/j.cclet.2024.109920.

References

[1] Y. Li, X.N. Ru, M. Yang, et al., Nature 626 (2024) 105–110.
[2] X.P. Shi, Y.P. Sun, Y.F. Shen, Science 373 (2021) 170.
[3] Y.J. Jiang, X.L. Hu, Electron 1 (2023) 15.
[4] D.L. Chao, W.H. Zhou, F.X. Xie, et al., Sci. Adv. 6 (2020) 4098.
[5] Y. Song, Q. Pan, H.Z. Lv, et al., Angew. Chem. Int. Ed. 60 (2021) 5718–5722.
[6] Y.Y. Zhao, C.T. Yang, Y.J. Yu, Chin. Chem. Lett. 35 (2024) 108865.
[7] Z.H. Wang, Y. Song, J. Wang, et al., Chem. Eng. J. 451 (2023) 2216290.
[8] R.Y. Wang, M.J. Shi, L.Y. Li, et al., Energy Environ. Sci. 9 (2016) 138652.
[9] L.F. Zhong, J. Li, C. Liu, et al., Adv. Funct. Mater. 33 (2023) 2215133.
[10] N. Patil, A. Mavrandonakis, C. Jérôme, et al., J. Mater. Chem. A 9 (2021) 505–514.
[11] F. Gámez, J.R. Avilés-Moreno, J. Martens, et al., J. Chem. Phys. 160 (2024) 094311.
[12] Z.P. Song, Y.M. Qian, T. Zhang, M. Otani, H.S. Zhou, Adv. Sci. 2 (2015) 1500124.

[13] J.H. Wang, Z.L. Liu, H.G. Wang, F.C. Cui, G.S. Zhu, Chem. Eng. J. 450 (2022) 138051.
[14] Y. Zhao, J. He, L.T. Hu, et al., Small 19 (2023) 2304182.
[15] Z.T. Zhang, M. Liao, H.Q. Lou, et al., Adv. Mater. 30 (2018) 1704261.
[16] D.F. Dang, D.H. Yu, E.G. Wang, Adv. Mater. 31 (2019) 1807019.
[17] X.Y. Zhao, Q. Liu, C.L. Zhong, et al., Adv. Funct. Mater. 32 (2022) 2205874.
[18] M. Zhou, M.Y. Liu, J. Wang, et al., Chem. Commun. 55 (2019) 6054.
[19] Y. Chen, J.Y. Li, Q. Zhu, et al., Angew. Chem. Int. Ed. 61 (2022) 2116289.
[20] Q. Zhao, W.W. Huang, Z.Q. Luo, et al., Sci. Adv. 4 (2018) 1761.
[21] Z.H. Li, J. Tan, X.D. Zhu, et al., Energy Storage Mater. 51 (2022) 294–305.
[22] Y. Kou, Y.H. Xu, Z.Q. Guo, D.L. Jiang, Angew. Chem. Int. Ed. 50 (2011) 8753–8757.
[23] V.A. Mihali, S. Renault, L. Nyholm, D. Brandell, RSC Adv. 4 (2014) 38004–38011.
[24] R.J. Shi, L.J. Liu, Y. Lu, et al., Adv. Energy Mater. 11 (2020) 2002917.
[25] H. Liang, R. Shi, Y. Zhou, et al., Chem. Commun. 58 (2022) 9536–9539.
[26] J. Qiao, M. Qin, Y.M. Shen, et al., Chem. Commun. 57 (2021) 4307–4310.
[27] T.J. Sun, H.H. Du, S.B. Zheng, et al., Small Methods 5 (2021) 2100367.
[28] M.H. Zhu, Li. Zhao, Q. Ran, et al., Adv. Sci. 9 (2022) 2103896.
[29] R. Emanuelsson, M. Sterby, M. Strømme, M. Sjödin, J. Am. Chem. Soc. 139 (2017) 4828–4834.
[30] X.L. Wang, J. Zhou, W.H. Tang, Energy Storage Mater. 36 (2021) 1–9.
[31] T.J. Sun, C. Liu, X.F. Xu, et al., J. Mater. Chem. A 8 (2020) 21983–21987.
[32] Z. Su, J.B. Chen, J. Stansby, et al., Small 18 (2022) 2201449.
[33] D. Alván, R. Grieco, N. Patil, et al., Batteries Supercaps 6 (2023) 2300023.
[34] K.B. Labasan, H.J. Lin, F. Baskoro, et al., ACS Appl. Mater. Interfaces 13 (2021) 17467–17477.
[35] Y. Mizuno, M. Okubo, E. Hosono, et al., J. Phys. Chem. C 117 (2013) 10877–10882.
[36] J. Chu, Z.L. Liu, J. Yu, et al., Angew. Chem. Int. Ed. 63 (2024) 2314411.
[37] M.J. Shi, J. He, Y. Zhao, et al., Mater. Des. 222 (2022) 111043.
[38] F. Ye, Q. Liu, H.L. Dong, et al., Angew. Chem. Int. Ed. 134 (2022) 2214244.
[39] T.J. Sun, W.J. Zhang, Q.S. Nian, Z.L. Tao, Chem. Eng. J. 452 (2022) 139324.
[40] K.S. Lakshmi, B. Vedhanarayanan, H.Y. Cheng, et al., J. Colloid Interface Sci. 619 (2022) 123–131.
[41] W.J. Zhang, M.Y. You, X.H. Yan, et al., Appl. Surf. Sci. 598 (2022) 153780.
[42] N.T. Chen, J. He, H.Y. Xuan, et al., Compos. Part B 270 (2024) 111145.
[43] Q. Li, B.Y. Wang, H.X. Zou, Q.F. Guo, G.M. Nie, J. Alloys Compd. 921 (2022) 166140.
[44] I. Marriam, Y.H. Wang, M. Tebyetekerwa, Energy Storage Mater. 33 (2020) 336–359.
[45] S.A. Hashemi, H.R. Naderi, S.M. Mousavi, et al., Carbon 188 (2022) 276–288.
[46] C. Strietzel, M. Sterby, H. Huang, et al., Angew. Chem. Int. Ed. 59 (2020) 9631–9638.
[47] K. Nueangnoraj, T. Tomai, H. Nishihara, T. Kyotani, I. Honma, Carbon 107 (2016) 831–836.
[48] Y. Xu, Y.T. Zheng, C.C. Wang, Q. Chen, ACS Appl. Mater. Interfaces 11 (2019) 23222–23228.
[49] Z.M. Qin, Y. Song, Y.Z. Liu, X.X. Liu, Energy Storage Mater. 53 (2022) 569–579.
[50] R.D. Cakan, M.R. Palacin, L. Croguennec, J. Mater. Chem. A 7 (2019) 20519–20539.
[51] N. Casado, D. Mantione, D. Shanmukaraj, D. Mecerreyes, ChemSusChem 13 (2020) 2464–2470.
[52] R.W. Mo, D. Rooney, K.N. Sun, H.Y. Yang, Nat. Commun. 8 (2017) 13949.
[53] Y.J. Dai, X.R. Yan, J.Z. Zhang, et al., Electrochim. Acta 442 (2023) 141870.
[54] Z.Z. Wu, P. Yang, S.Y. Wang, S. Li, S.Q. Zhang, Trends Chem. 4 (2022) 1121–1134.
[55] T.J. Sun, H.H. Du, S.B. Zheng, J.Q. Shi, Z.L. Tao, Adv. Funct. Mater. 31 (2021) 2010127.
[56] S.Y. Dong, N. Lv, R.Q. Ren, et al., Sci. China Mater. 65 (2022) 3069–3076.
[57] L.C. Tong, Y. Jing, R.G. Gordon, M.J. Aziz, ACS Appl. Energy Mater. 2 (2019) 4016–4021.
[58] N. Lv, R.Q. Ren, Y.L. Wu, et al., Electrochim. Acta 431 (2022) 141097.